Cell Reports, Volume *29*

Supplemental Information

An Excitatory and Epileptogenic Effect of Dentate Gyrus Mossy Cells in a Mouse Model of Epilepsy

Justin J. Botterill, Yi-Ling Lu, John J. LaFrancois, Hannah L. Bernstein, David Alcantara-Gonzalez, Swati Jain, Paige Leary, and Helen E. Scharfman

Supplemental Information

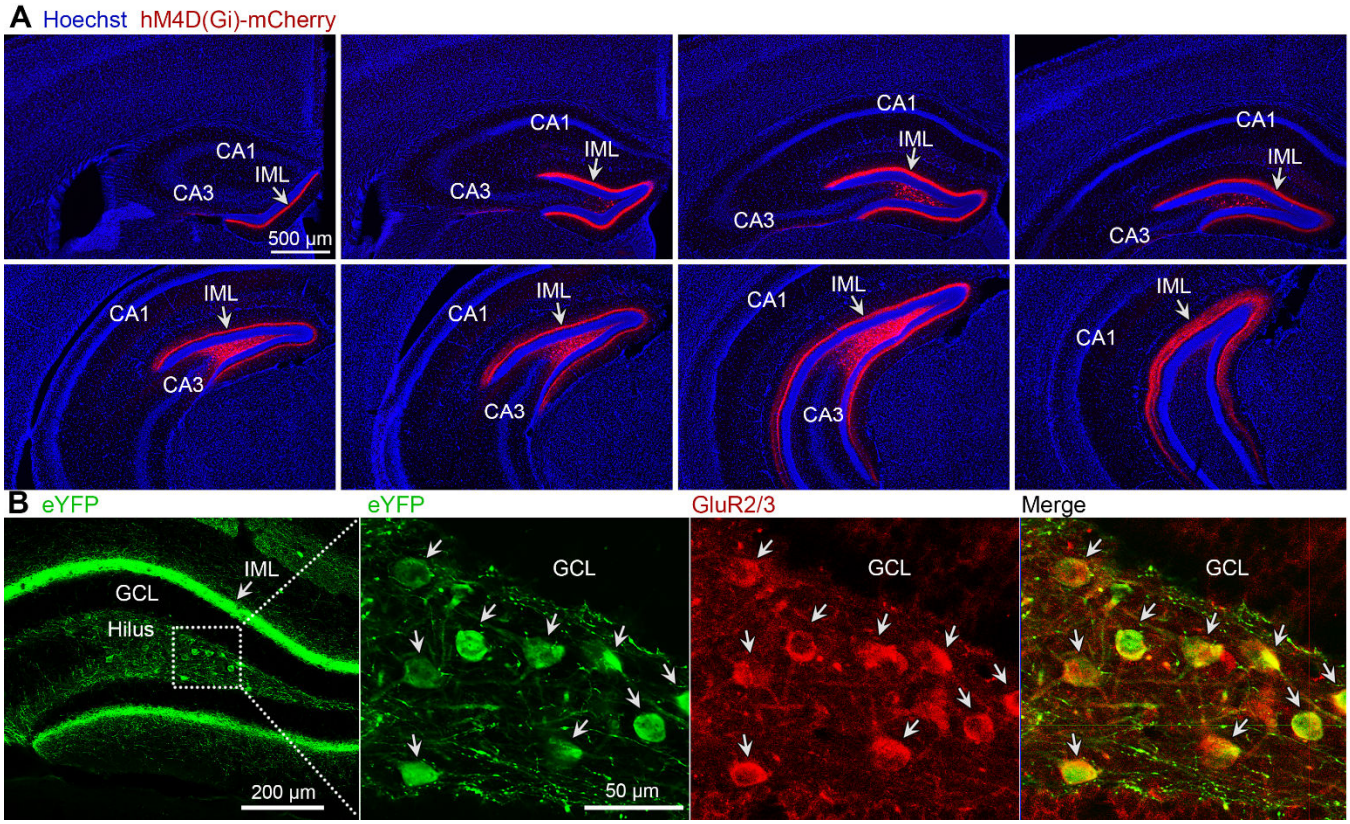

Figure S1. DrD2-Cre mice exhibit viral expression preferentially in MCs and their axons. Related to Figures 1, 4, and 6.

(A) Representative AAV-hSyn-DIO-hM4D(Gi)-mCherry expression in a DrD2-Cre$^{+/-}$ mouse injected with virus in the dorsal and ventral hippocampus, bilaterally (as shown in Figure 1). Sections were counterstained with Hoechst to visualize the hippocampal cell layers. In sections proximal to the injection sites, mCherry expression is localized to the hilus. We estimate that <50% of all MCs in the DG were labeled in these experiments (*n*=5). However, mCherry-expressing MC axons densely innervate the IML (arrows) across the septotemporal axis of the DG, consistent with the location of MC axons (Amaral et al., 2007; Buckmaster et al., 1996; Scharfman and Myers, 2012). Scale bar: 500 µm.

(B) DrD2-Cre$^{+/-}$ mice were injected with AAV-EF1α-DIO-eYFP in the hippocampus and sections near the injection site were stained to detect colocalization with GluR2/3 (5-7 sections per mouse, 50 µm thick sections; *n*=5 mice). The vast majority hilar eYFP-expressing cells colocalized with GluR2/3 (1199/1240 cells=96.7%; arrows), consistent with the finding that MCs are the primary hilar cell type labeled with GluR2/3 (Scharfman and Myers, 2012). Scale bars: 200 µm and 50 µm.

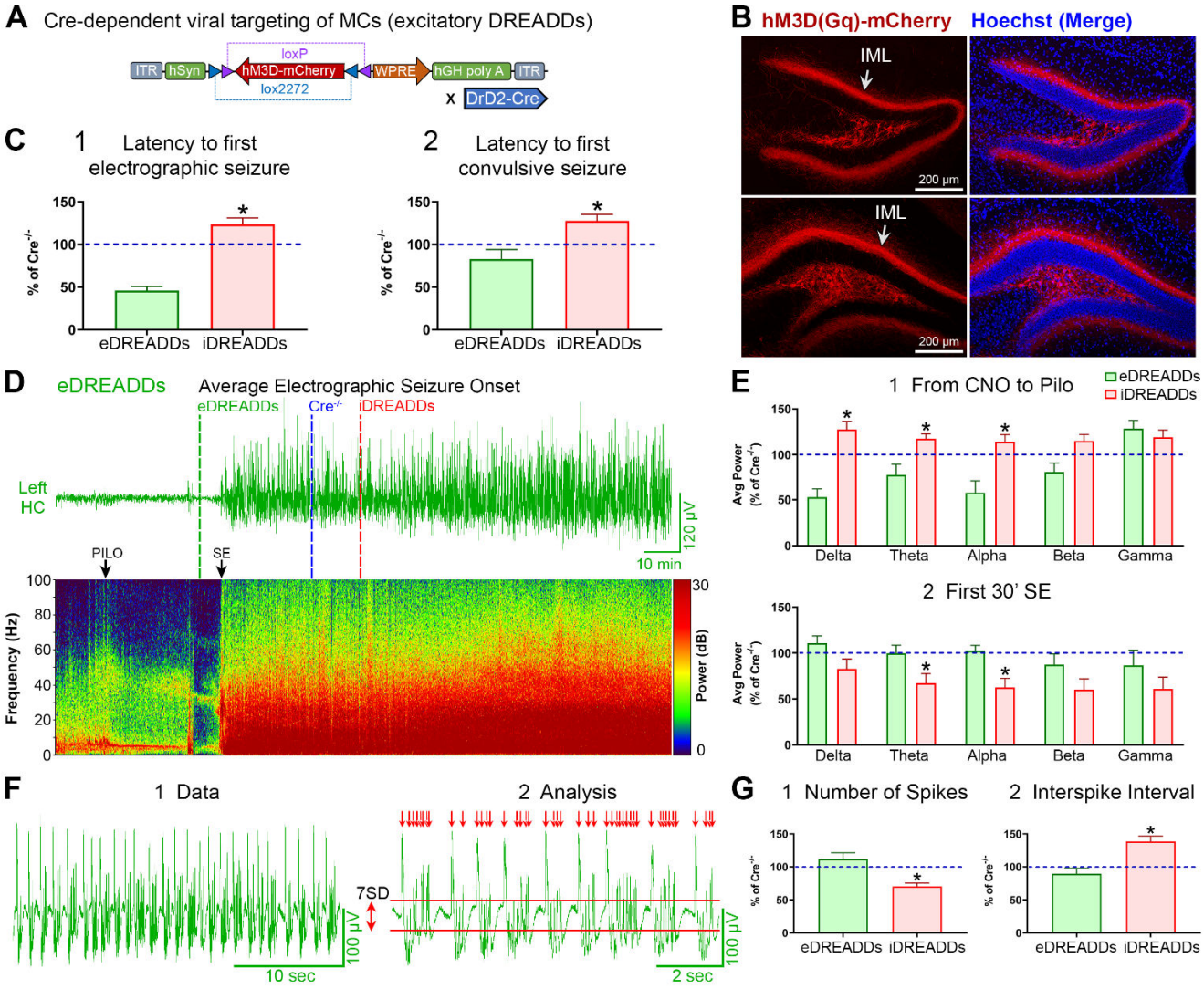

Figure S2. Enhancing MC activity with eDREADDs during SE has opposing effects compared to iDREADDs. Related to Figures 1 and 2.

(A) For selective excitation of MCs, the Cre-dependent eDREADD AAV-hSyn-DIO-hM3D(Gq)-mCherry was injected into the dorsal and ventral hippocampus, bilaterally.

(B) Representative hM3D(Gq)-mCherry expression in the hilus and IML (arrows). Scale bars: 200 µm.

(C) eDREADDs and iDREADDs mice were significantly different in their latency to seizure onset (two-way ANOVA, $F(1,36)=23.88$, $p<0.001$; Bonferroni post-hoc tests, C1 $p<0.001$, C2 $p=0.018$).

(D) Representative EEG trace and corresponding spectrogram showing pilocarpine injection and SE onset. The vertical dashed lines mark the mean latency to electrographic seizures for eDREADDs (green line), Cre$^{-/-}$ (blue), and iDREADDs (red) mice. Note the remarkably faster electrographic seizure latency in eDREADDs mice.

(E1) EEG power during the CNO period in eDREADDs vs. iDREADDs mice was significantly different (two-way ANOVA, $F(1,90)=35.78$, $p<0.001$). Post-hoc analyses revealed significant differences in delta ($p<0.001$), theta ($p<0.001$), and alpha ($p=0.039$) power.

(E2) During SE onset, power in eDREADDs and iDREADDs mice was significantly different (two-way ANOVA, $F(1,90)=18.85$, $p<0.001$) with significantly reduced power in iDREADDs mice in theta ($p=0.002$) and alpha ($p=0.028$) frequencies but no other bands (all p values >0.087).

(F) *1-2.* EEG trace showing representative spiking during SE onset.

(G1) The number of spikes during SE onset was significantly reduced in iDREADDs compared to eDREADDs mice ($t(18)=3.626$, $p=0.001$).

(G2) The interval between spikes (interspike interval) was significantly greater in iDREADDs than eDREADDs mice ($t(18)=2.416$, $p=0.026$). To illustrate the opposing effects of eDREADDs vs. iDREADDs, relative to no MC manipulation (i.e., Cre$^{-/-}$), all graphs are presented as the percentage of the Cre$^{-/-}$ mean (indicated by the horizontal dashed blue line) ± SEM. *p<0.05.

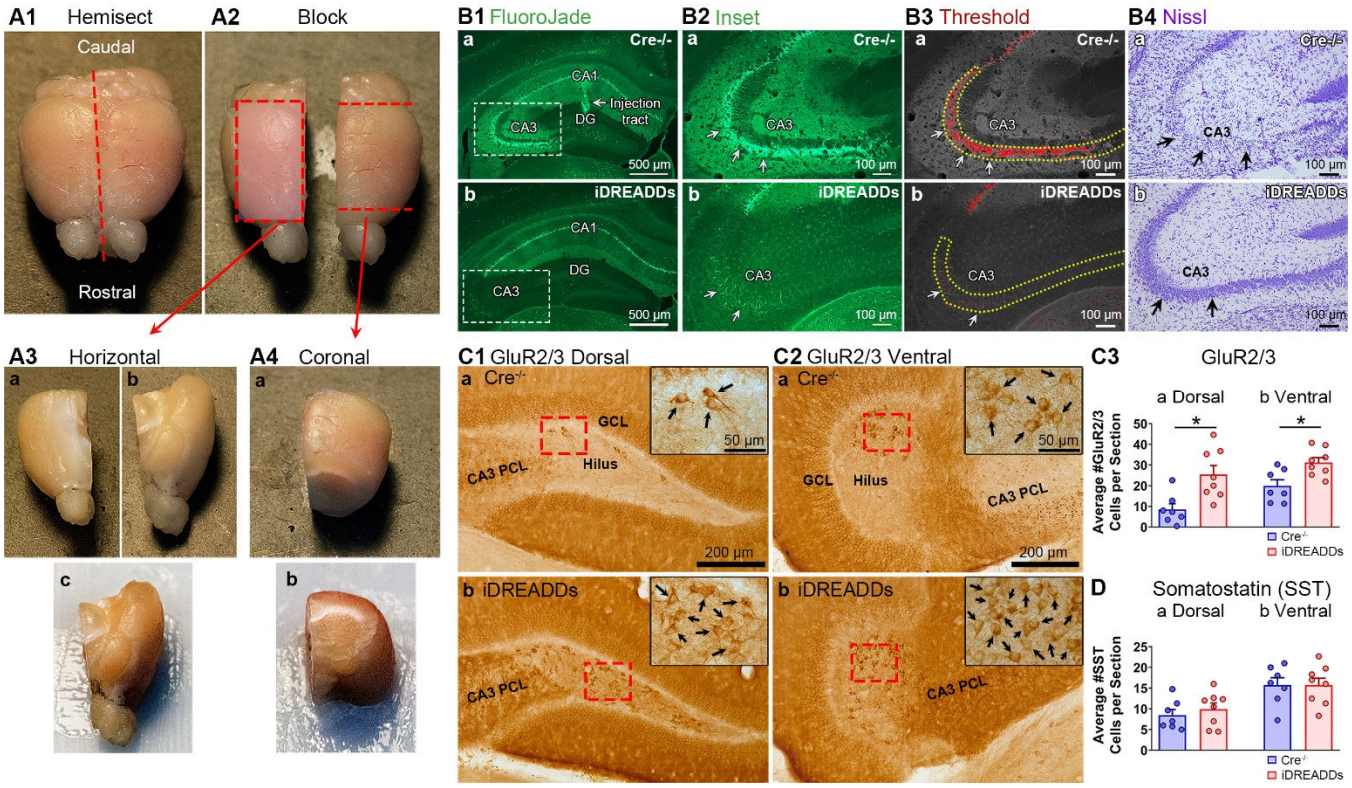

Figure S3. Anatomical methods and quantification. Related to Figure 4.
(A1 and A2) Perfusion-fixed brains were hemisected and blocked (red dashed lines).
(A3) The dorsal surface of the right hemisphere was (A3a) trimmed flat and then (A3b) glued with the dorsal surface facing down for (A3c) sectioning in the horizontal plane.
(A4a) The left hemisphere was blocked prior to (A4b) sectioning in the coronal plane. Sectioning in both planes allowed maximal visualization of the hilus in dorsal and ventral locations.
(B1) Representative FluoroJade staining in $Cre^{-/-}$ and iDREADDs mice.
(B2) Insets of CA3 from B1a and B1b shown at high magnification.
(B3) Photomicrographs of FluoroJade staining were converted to grayscale using ImageJ. The ImageJ threshold function was used to calculate the area fraction of FluoroJade staining (red; arrows) within the traced contour around the CA3 cell layer (yellow dotted lines). Note the greater FluoroJade staining in $Cre^{-/-}$ mice (arrows).
(B4) The pattern of CA3 FluoroJade staining was consistent with CA3 cell loss observed in adjacent Nissl-stained sections (compare arrows in B4a showing no detectable neuronal cell bodies with B4b where numerous cell bodies are present). Scale bars: 500 µm and 100 µm.
(C1 and C2) Representative GluR2/3 staining in dorsal and ventral sections of $Cre^{-/-}$ (a) and iDREADDs (b) mice. Insets of the boxed area (red) show GluR2/3-ir hilar cells. Scale bars: 200 µm and 50 µm.
(C3a and C3b) iDREADDs mice had significantly more hilar GluR2/3 cells per section in both dorsal and ventral DG compared to $Cre^{-/-}$.
(D) Adjacent sections processed using an antibody to somatostatin revealed no detectable group differences.
Data are represented as mean ± SEM. *$p<0.05$.

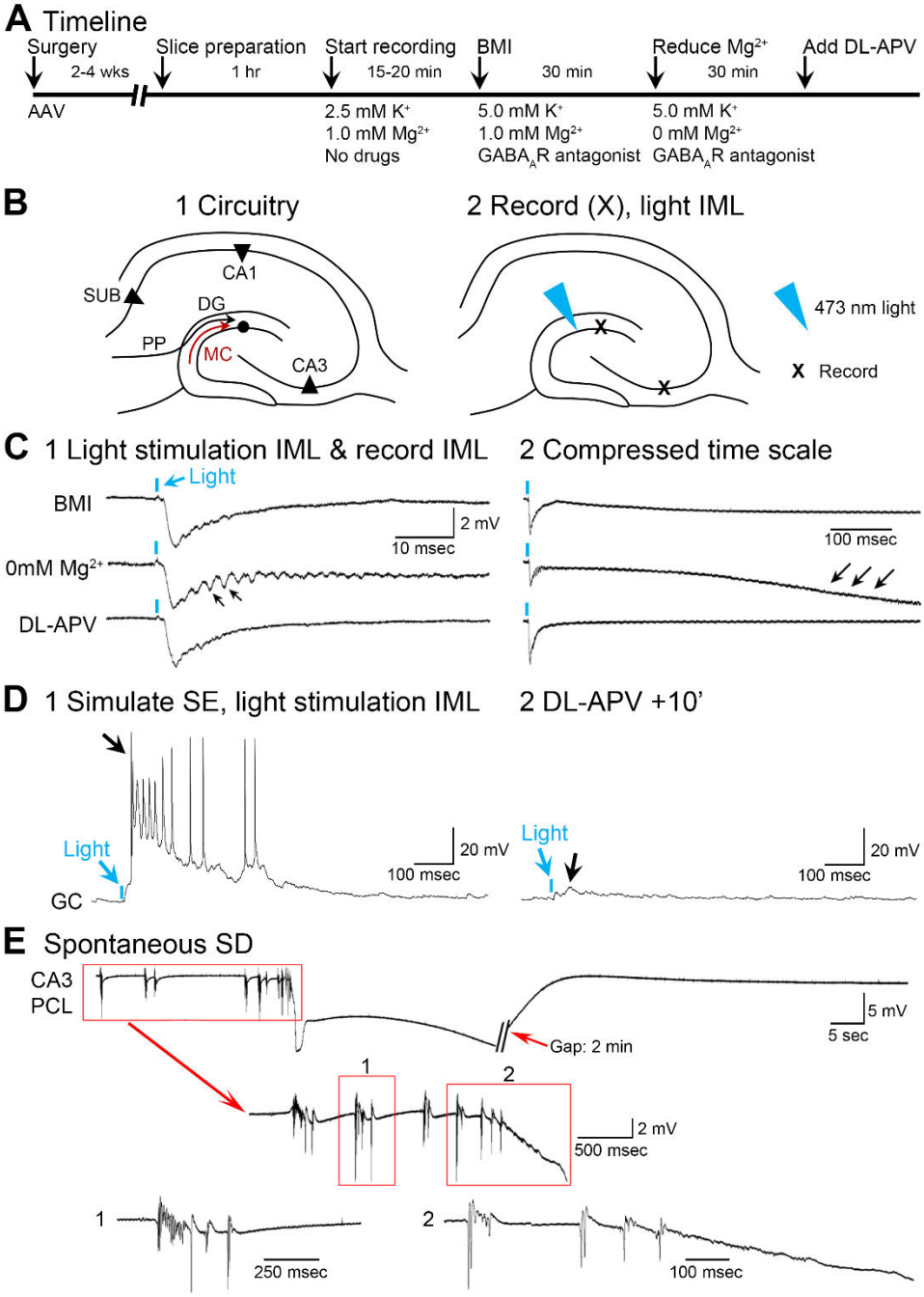

Figure S4. During a slice simulation of SE, optogenetic activation of MC axons can trigger a severe seizure-like event: spreading depolarization (SD) dependent on NMDA receptors. Related to Figures 6 and 7.
(A) Timeline. AAV-EF1α-DIO-hChR2(H134R)-eYFP was injected in the left hippocampus and 2-4 wks later distal slices with ChR2 expression in MC axons were used. Baseline recordings confirmed the light response was stable and then SE was partly simulated by blocking $GABA_A$ receptors with BMI and raising $[K^+]$ to 5 mM. Later, $[Mg^{2+}]$ in the ACSF was reduced to nominally 0 mM. and then DL-APV was added to address the role of NMDA receptors.
(B1) Schematic of DG circuitry in slices distal to the viral injection.
(B2) 473 nm light was aimed at the IML and extracellular recordings were made in the IML (to record field potentials or field EPSPs) or the CA3 cell layer.
(C1) A single light pulse after $GABA_A$ receptor block resulted in larger fEPSPs. Notably, after $[Mg^{2+}]_o$ was reduced, the light pulse evoked fEPSPs with population spikes (C1, black arrows) that triggered SD (C2, black arrows). DL-APV reduced the population spikes and prevented subsequent light-evoked SD.
(D1) During simulated SE, a single light pulse to the IML evoked paroxysmal depolarization shifts (PDSs) in patched GCs.
(D2) Bath application of DL-APV significantly attenuated the light-evoked response (black arrow).
(E) Example of a spontaneous SD recorded in the CA3 PC layer in another type of experiment, showing that SD onset is characterized by a slow DC (direct current) negative shift similar to the SD following the response to light in C2.

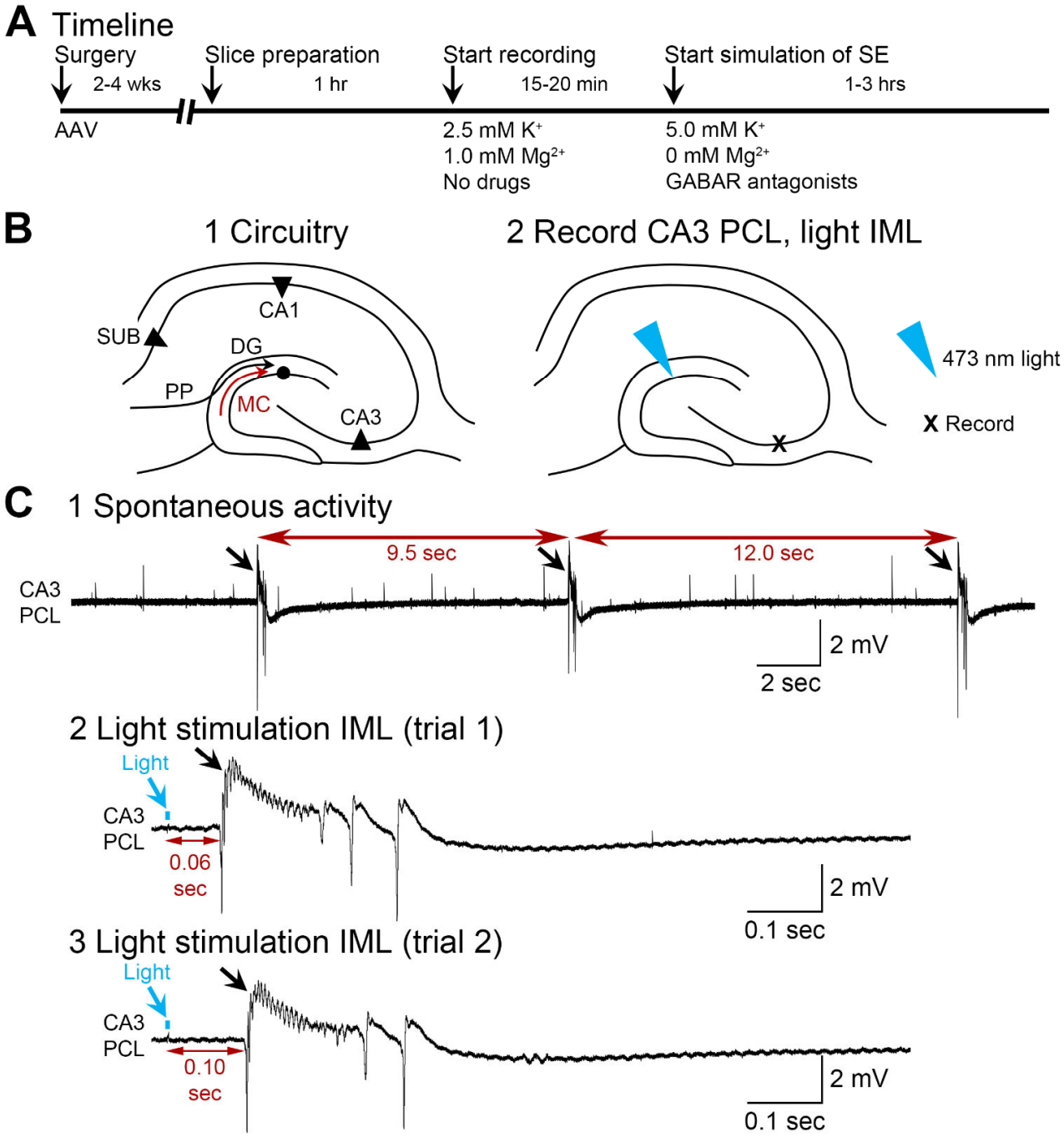

Figure S5. Spontaneous CA3 bursts are intermittent whereas light-evoked bursts occur at a short latency. Related to Figure 7.

(A) Timeline. AAV-EF1α-DIO-hChR2(H134R)-eYFP was injected into the left hippocampus and 2-4 wks later slices were selected distal to the injection site, with ChR2 expression in MC axons.

(B1) Schematic of DG circuitry.

(B2) 473 nm light was aimed at the IML and extracellular field potentials were recorded in the CA3 pyramidal cell layer (black arrows).

(C1). During simulated SE, spontaneous CA3 bursts were detected at regular intervals (~one every 10 sec; black arrows).

(C2) A brief light pulse (2 msec; blue arrow) reliably triggered a CA3 burst ≥ 1 order of magnitude faster (<0.1 sec; red arrows) than the shortest spontaneous interburst interval. Note that optical stimulation of areas outside the DG did not evoke a burst.

(C3) A second light pulse showed the same result where a CA3 burst was evoked with a very short latency (red arrows). These data suggest that MC stimulation evoked bursts and they were not spontaneous CA3 bursts.

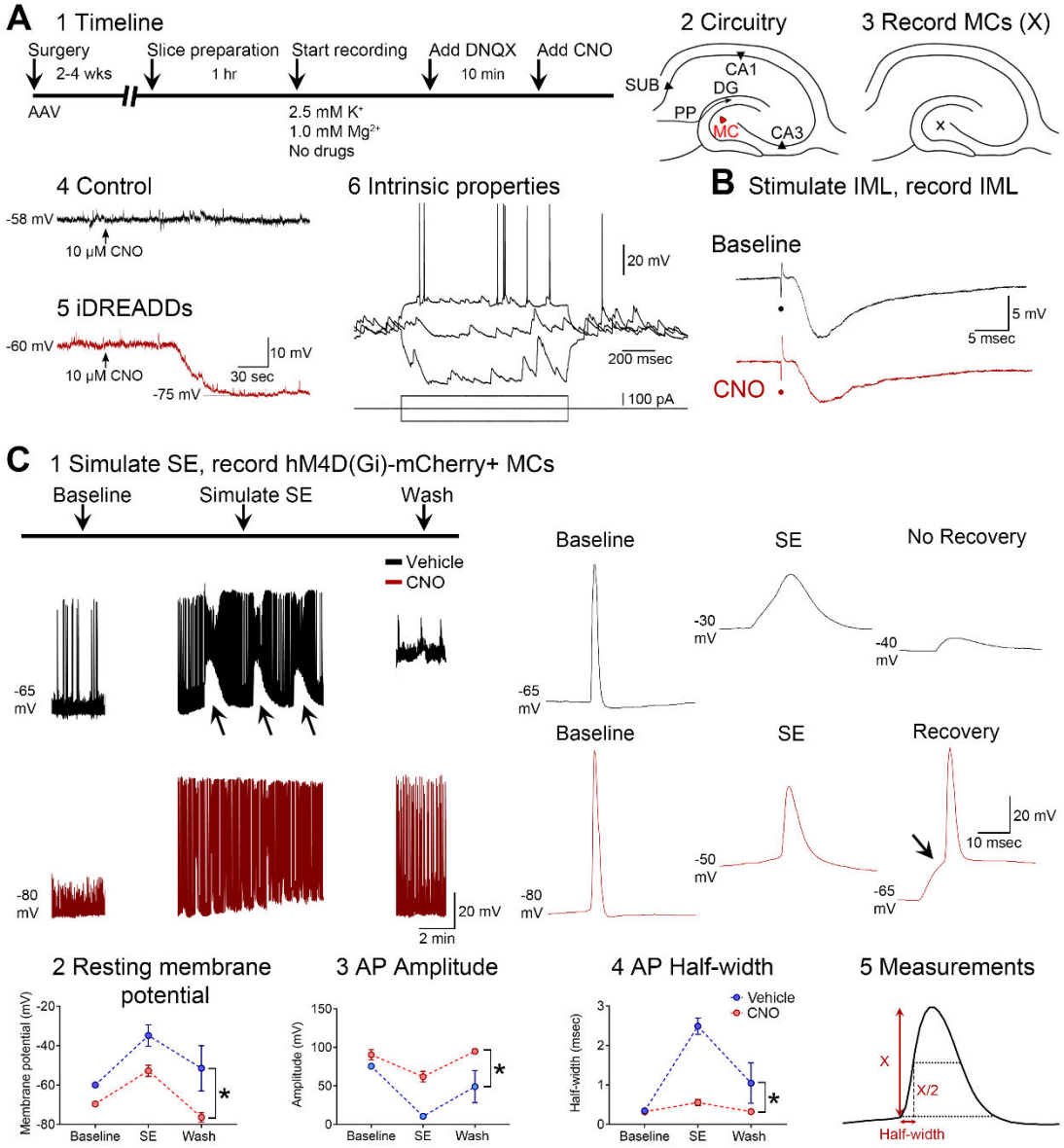

Figure S6. MCs that express hM4D(Gi)-mCherry are inhibited by CNO *in vitro*. Related to Figure 1.
(A1) Timeline. AAV-hSyn-DIO-hM4D(Gi)-mCherry was injected into the hippocampus and 2-4 wks later slices were made. DNQX (10 μM) was added to the buffer prior to CNO to reduce spontaneous activity of MCs.
(A2) Schematic of DG circuitry.
(A3) Recordings were made in the hilus near the viral injection site so that fluorescent MCs could be patched.
(A4) CNO had no effect on MCs without hM4D(Gi) expression (n=6 cells in 4 mice).
(A5) MCs with hM4D(Gi)-mCherry expression hyperpolarized in response to CNO (8.00 ± 1.67 mV; n=6 cells in 4 mice).
(A6) Intrinsic properties identified the patched cells as MCs, with criteria discussed elsewhere (Scharfman and Myers, 2012).
(B) To evaluate the network effects of MC inhibition, MC axons were electrically stimulated in the IML and the evoked fEPSP in the IML was recorded. Bath application of CNO (10 μM) depressed the evoked fEPSP (n=3 slices in 3 mice).
(C1) MCs expressing hM4D(Gi)-mCherry were sliced, each slice was pre-treated with vehicle (n=3 cells) or CNO (10 μM; n=3 cells) and then MCs were patched and the slice underwent simulated SE. CNO resulted in more hyperpolarized resting potentials compared to vehicle. Once simulated SE was initiated, MCs rapidly depolarized and ictal-like events occurred in the slice and MCs (arrows). After substantial depolarization (shown on the left) action potential (AP) amplitude decreased, while the AP half-width increased (see traces on the right). Remarkably, CNO minimized the adverse effects on AP amplitude and half-width during simulated SE. After washout, vehicle-treated MCs showed a poor recovery, whereas MCs treated with CNO recovered more. Arrow at the far right points to a spontaneous EPSP with an AP at its peak.
(C2 to C4) Quantified data for baseline, SE, and washout periods. Repeated two-way ANOVAs revealed that CNO-treated MCs differed from control MCs in RMP (F(1,4)=9.69, p=0.003), AP amplitude (F(1,4)=24.92, p=0.007), and AP half-width (F(1,4)=56.03, p=0.001).
(C5) Amplitude was measured as indicated by X; half-width was measured as indicated by the time between AP onset and half the peak AP amplitude. Data are represented as mean ± SEM. *p<0.05.

Simulation of SE Onset				
Drug Name	**Vendor**	**Solvent**	**Stock Conc.**	**Final Conc.**
Bicuculline Methiodide (BMI)	Sigma	0.9% NaCl	10 mM	10 µM (Interface) 20 µM (Submerge)
CGP52432	Sigma	ddH_20	5 mM	10 µM
4-Aminopyridine (4-AP)	Sigma	ddH_20	100 mM	100 µM
Other drugs				
Drug Name	**Vendor**	**Dissolved in**	**Stock Conc.**	**Working Conc.**
Clozapine N-oxide (CNO)	Enzo Life Sciences	0.9% NaCl	10 mM	10 µM
DL-APV	Sigma	ddH_20	10 mM	50 µM
DCG-IV	Tocris	ddH_20	10 mM	2 µM
DNQX	Tocris	Dimethyl sulfoxide	50 mM	10 µM

Table S1. List of drugs used in slice experiments. Related to Figures 6, 7, S4, S5, S6.
In slices (Figures 6, 7, S4, S5, S6), SE onset was simulated by adding GABA receptor antagonists and using ACSF with 5 mM KCl and 0 mM $MgSO_4$. In some experiments (described in the text), 4-AP was added.

Note that light-evoked PDSs in GCs were demonstrated in additional experiments where drugs were added sequentially rather than simultaneously (e.g. Figure 6, Figure S4). Notably, the sequential approach showed that removing $MgSO_4$ from the ACSF had a large effect, i.e., optical stimulation evoked ≤ 2 APs in the presence of GABA receptor antagonists and 5 mM $[K^+]_o$, whereas, the same optical stimulus evoked prolonged firing (PDSs) after removal of $[Mg^{2+}]_o$ also (*n*=3 slices in 3 mice). Optical stimulation could also evoke SD after reducing $[Mg^{2+}]_o$ but not before, suggesting a major effect of NMDA receptors, which was addressed using the competitive NMDA receptor antagonist DL-APV (50 µM; Figure S4).

To activate iDREADDs in slices, 10 µM CNO was used as reported elsewhere (Gallo et al., 2018; Katzel et al., 2014). The metabotropic glutamate receptor type II agonist DCG-IV (1-2 µM) was used to block mossy fiber transmission preferentially.